Effect of Chromium Substitution on the Lattice Vibration of Spinel Lithium Manganate: A New Interpretation of the Raman Spectrum of $LiMn_2O_4$

Seong-Ju Hwang,*,† Dae-Hoon Park,† Jin-Ho Choy,‡ and Guy Campet§

Department of Applied Chemistry and Center for Emerging Wireless Transmission Technology, College of Natural Sciences, Konkuk University Chungju Campus, Chungju, Chungbuk 380-701, Korea, National Nanohybrid Materials Laboratory, School of Chemistry and Molecular Engineering, Seoul National University, Seoul 151-747, Korea, and Institut de Chimie de la Matière Condensée de Bordeaux (ICMCB) du CNRS, Château Brivazac, Avenue du Dr. A. Schweitzer, 33608 Pessac, France

Received: September 8, 2003; In Final Form: June 21, 2004

The variation of the lattice vibration of spinel lithium manganate upon chromium substitution has been investigated by performing a combinative micro-Raman and X-ray absorption spectroscopic (XAS) analysis. As the manganese ion in the spinel $LiMn_{2-x}Cr_xO_4$ is replaced by a chromium ion, the relative intensities of two main Raman peaks at ~580 and ~620 cm^{-1} are remarkably changed. This change cannot be understood by the previous peak assignment on the basis of the average crystal structure of the cubic spinel lattice. According to the Mn K-edge XAS analysis, it is certain that there are two kinds of local structures around the manganese in the spinel $LiMn_{2-x}Cr_xO_4$ and the substitution of Mn with Cr gives rise to a depression of the local tetragonal distortion around the manganese ion. On the basis of this finding, we are able to re-interpret two main Raman features of the cubic spinel lithium manganate as totally symmetric A_{1g} modes without and with tetragonal distortion, respectively. This new interpretation is further supported not only by the comparison with the reference spectra of λ-MnO_2 and $Li_2Mn_2O_4$ but also by the good correlation between the ratio of Mn^{+IV}/Mn^{+III} concentration and the relative intensities of two Raman peaks.

Introduction

The spinel structured lithium manganese oxides have attracted intense research interest as alternative cathode materials for rechargeable lithium batteries.[1] Although they possess economic and ecological merits over commercialized $LiCoO_2$, a remarkable capacity loss during electrochemical charge−discharge process frustrates the commercial use of this material. For this reason, many attempts have been made to improve the electrochemical performance of this compound.[2−5] As a result, it was well documented that the partial substitution of manganese ions with other transition metal ions such as Cr^{+III} and Co^{+III} enhances the cyclability of the $LiMn_2O_4$ spinel.[5] To understand such an improvement of electrochemical performance, various spectroscopic methods including conventional diffraction tools have been applied for examining the effect of cation substitution on the crystal structure of the spinel lithium manganate.[6−12] Recently Raman spectroscopy has received special attention as a powerful way of studying lithium manganese oxides with closely related crystal structures, because it is very sensitive to the variation of crystal symmetry.[10−15] However, only limited numbers of Raman studies on spinel lithium manganates have been reported.[10−12] This would be due to difficulties in interpreting the Raman spectra of such complex-structured inorganic solids. Previously it was reported that the cubic spinel $LiMn_2O_4$ shows several Raman features corresponding to Mn−O and Li−O vibration modes.[10−12] The observed Raman peaks were assigned on the basis of the theoretical calculation with the average crystal structure obtained from X-ray crystallography.[10] However, taking into account the fact that Raman features are very sensitive to a dynamic local structural deformation,[15] it is rather problematic to interpret the Raman spectra based on a static average crystal structure. In fact, there have been several reports about the charge disproportionation of manganese ion and the dynamic tetragonal distortion in $LiMn_2O_4$.[16,17]

In this study, we have examined the local crystal structure of the $LiMn_{2-x}Cr_xO_4$ spinel compounds by performing combinative micro-Raman and X-ray absorption (XAS) spectroscopy, to understand the variation of the lattice vibration of the spinel lithium manganate upon Cr substitution. On the basis of the information about the local atomic arrangement, we were able to re-interpret the Raman spectrum of the spinel $LiMn_2O_4$. This new interpretation was further confirmed not only by comparing with the reference spectra of λ-MnO_2 and $Li_2Mn_2O_4$ but also by plotting the ratio of Mn^{+IV}/Mn^{+III} concentration and the relative intensities of two main Raman peaks.

Experimental Section

The spinel $LiMn_{2-x}Cr_xO_4$ ($0 \le x \le 0.5$) samples were prepared by using a conventional solid-state reaction method.[3] The crystal structures of these materials were studied by X-ray diffraction (XRD) measurement using Ni-filtered Cu Kα radiation with a graphite diffracted beam monochromator. The lattice parameters were determined by Rietveld analysis. As summarized in Table 1, it becomes clear that the replacement of Mn with Cr has no influence on the overall crystal symmetry of the spinel compounds. However, the Cr substitution leads to a contraction of the unit cell, which can be understood in light of the fact that Mn^{+III} ion is replaced partly by relatively smaller

* To whom all correspondences should be addressed. Tel: +82-43-840-3569. Fax: +82-43-851-4169. E-mail: hwangsju@kku.ac.kr.
† Konkuk University Chungju Campus.
‡ Seoul National University.
§ Institut de Chimie de la Matière Condensée de Bordeaux (ICMCB) du CNRS.

10.1021/jp036683x CCC: $27.50 © 2004 American Chemical Society
Published on Web 07/31/2004

TABLE 1: Lattice Parameters, Unit Cell Volumes (V_c), Crystal Symmetries, and Chemical Formulas of Lithium Manganese Oxides

nominal formula	a (Å)	c (Å)	V_c	crystal symmetry	chemical formula
$LiMn_2O_4$	8.248		561.013	cubic	$Li_{0.99}Mn_2O_4$
$LiMn_{1.9}Cr_{0.1}O_4$	8.239		559.263	cubic	$Li_{1.04}Mn_{1.87}Cr_{0.13}O_4$
$LiMn_{1.8}Cr_{0.2}O_4$	8.229		557.239	cubic	$Li_{0.99}Mn_{1.76}Cr_{0.24}O_4$
$LiMn_{1.7}Cr_{0.3}O_4$	8.224		556.189	cubic	$Li_{1.05}Mn_{1.67}Cr_{0.33}O_4$
$LiMn_{1.5}Cr_{0.5}O_4$	8.211		553.603	cubic	$Li_{1.10}Mn_{1.47}Cr_{0.53}O_4$
λ-MnO_2	8.040		519.718	cubic	$Li_{0.03}MnO_2$
$Li_2Mn_2O_4$	5.659	9.291	297.538	tetragonal	$Li_{2.34}Mn_2O_4$

Cr^{+III} ion (Mn^{+III} (6) = 0.785 Å, Cr^{+III} (6) = 0.755 Å, where the number in parentheses represents the coordination number[18]). The delithiation of the lithium manganate was achieved through the reaction with aqueous 2.5 M H_2SO_4 solution, whereas the lithiation reaction was performed by using 1.6 M *n*-BuLi solution in hexane.[3]

The micro-Raman spectra presented here were recorded on a Dilor-Omars microspectrometer coupled with an optical microscope (spatial resolution of 1 μm^2) and an intensified 1024-channel photodiode array detector. The samples were excited with the 514.5 nm line of an Ar^+ laser. All the present spectra were obtained by backscattering from the powdered sample or the freshly cleaved surfaces of polycrystalline sample. The resolution of the present spectra was 3−4 cm^{-1}. By adopting a diode laser (λ = 785 nm) as an excitation source, we have also measured the Raman spectra of the cubic spinel $LiMn_{1.5}Cr_{0.5}O_4$ to check out the dependence of the Raman spectra of the Cr-substituted compounds on the laser frequency. A slight change of spectral features was observed, suggesting the absence of a resonance Raman effect in these compounds. This coincides with the previous report regarding the negligible wavelength dependency of the cubic spinel lithium manganate.[10] To prevent possible thermal damage of the sample, the power of the incident laser light was maintained at lower than 5 mW. After each measurement, the sample surface was thoroughly checked to remove the possibility of spectral modification caused by the surface degradation. The peak areas of Raman features were estimated by convoluting the spectra with Lorentzian functions.

XAS experiments were carried out by using the extended X-ray absorption fine structure (EXAFS) facility installed at the beam line 7C at the Photon Factory in Tsukuba.[19] The XAS data were collected at room temperature in a transmission mode using gas-ionization detectors. All the present spectra were calibrated by measuring the spectrum of Mn metal foil. The data analysis for the experimental spectra was performed by using the standard procedure reported previously.[20] To probe the existence of the dynamic tetragonal distortion in $LiMn_{2-x}Cr_xO_4$, we have carried out a quantitative EXAFS analysis by constructing multiple Mn−O bond models consisting of two Mn−O bonding pairs and one Mn−Mn bonding pair. And the obtained fitting results were compared with those calculated with single Mn−O bond models. In the course of fitting analysis, the coordination number (CN) was fixed to the crystallographic values whereas the amplitude reduction factor (S_0^2) was allowed to vary. The best-fit S_0^2's of all the present $LiMn_{2-x}Cr_xO_4$ compounds are consistent with one another within 10% deviation. All the bond distances (R), Debye−Waller factors (σ^2), and energy shifts (ΔE) were set as variables. In case of the multiple Mn−O bond models, ΔE was constrained to be identical for two Mn−O coordination shells, which can be rationalized from the fact that adjacent shells consisting of the same atoms would possess a very similar degree of energy shift.

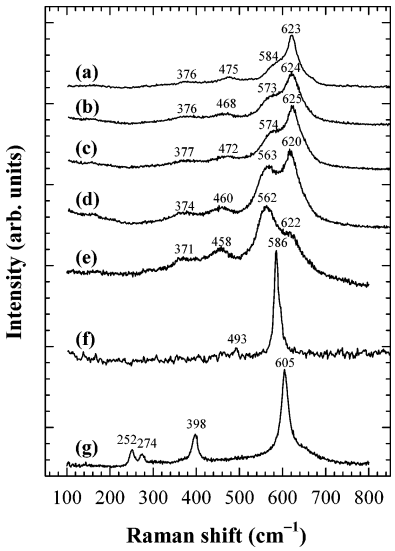

Figure 1. Micro-Raman spectra for the chromium-substituted $LiMn_{2-x}Cr_xO_4$ spinel compounds with x = (a) 0, (b) 0.1, (c) 0.2, (d) 0.3, and (e) 0.5, and for the references (f) cubic spinel λ-MnO_2 and (g) tetragonal spinel $Li_2Mn_2O_4$.

Results and Discussion

The micro-Raman spectra of the cubic spinel $LiMn_{2-x}Cr_xO_4$ ($0 \le x \le 0.5$) are presented in Figure 1, together with those of cubic spinel λ-MnO_2 and tetragonal spinel $Li_2Mn_2O_4$ compounds. Although factor group analysis predicts five Raman active modes ($A_{1g} + E_g + 3T_{2g}$) for the cubic spinel $LiMn_2O_4$,[10] only four Raman peaks are discernible in the present spectra. Except for the absence of several weak features, the overall spectral feature appears to be very close to the previously reported ones.[10−12,21] According to the theoretical calculation based on the average crystal structure of $LiMn_2O_4$,[10] the strongest peak around 620 cm^{-1} was interpreted as a symmetric A_{1g} mode whereas the other phonon lines at ∼370, ∼470, and ∼580 cm^{-1} were assigned as $T_{2g}(1)$, $T_{2g}(2)$, and $T_{2g}(3)$ modes, respectively. In addition, a very weak and diffuse peak that is absent in the present spectra, was identified at 432 cm^{-1} and assigned as the E_g mode.[10] As shown in Figure 1, the substitution of Mn with Cr gives rise to a remarkable variation of the Raman spectra, that is, the intensity change of two strong features at around 580 and 620 cm^{-1}. As the Cr content increases, the peak at ∼620 cm^{-1} is depressed whereas the peak at ∼580 cm^{-1} is enhanced. At the present highest substitution rate of x = 0.5, the intensity of the former peak becomes smaller than that of the latter. Because the Cr substitution has no influence on the space group of the given spinel compound,[3] Raman-active phonon modes should remain unchanged regardless of the Cr content. Moreover, judging from the fact that all the Raman-active modes are related not to the vibration of transition metal but to those of oxygen and lithium,[10] there is no reasonable origin for the marked increase of $T_{2g}(3)$ phonon line caused by the replacement of Mn with Cr. Therefore the observed spectral change upon Cr substitution cannot be understood on the basis of the previous assignment.[10] This suggests strongly the dynamic deformation of the local structure upon Cr substitution that cannot be detected by conventional diffraction tools.

In this regard, the local atomic arrangement of Cr-substituted derivatives has been investigated by using XAS analysis. The Mn K-edge X-ray absorption near-edge structure (XANES) spectra for $LiMn_{2-x}Cr_xO_4$ (x = 0, 0.2, and 0.5) are shown in Figure 2,[22] in comparison with the reference spectra of cubic spinel λ-MnO_2 and tetragonal spinel $Li_2Mn_2O_4$. All the present

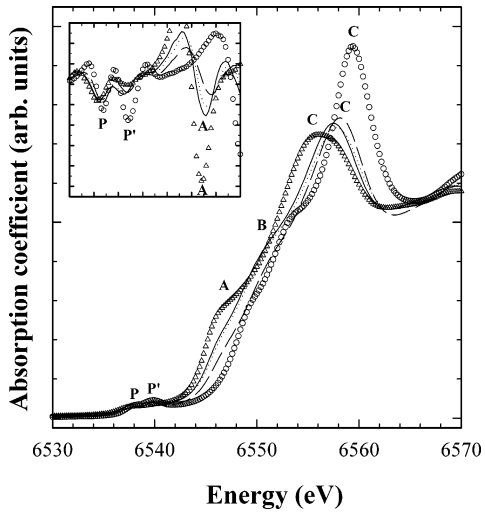

Figure 2. Mn K-edge XANES spectra for the spinel $LiMn_{2-x}Cr_xO_4$ compounds with $x = 0$ (solid lines), 0.2 (dotted lines), and 0.5 (dashed lines) and the references cubic spinel λ-MnO_2 (circles) and tetragonal spinel $Li_2Mn_2O_4$ (triangles). The corresponding second derivative spectra in the energy range of 6535−6549 eV are presented in the inset.

samples exhibit a small preedge peak P corresponding to the dipole-forbidden 1s → 3d transition, which indicates the octahedral symmetry around the manganese ion. This preedge peak is displaced toward higher energy side with increasing the Cr concentration, highlighting the increase of the average Mn oxidation state. This is in good agreement with the blue shift of the edge jump induced by the replacement of Mn with Cr. In the main-edge region, there are several features corresponding to the dipole-allowed transitions from core 1s to the unoccupied 4p levels. Among them, peak A has been assigned as $1s \rightarrow 4p_\pi$ transition with a shakedown process in the trivalent manganese ion.[23] Because the shakedown process is sensitive to the electrostatic repulsion between $4p_\pi$ orbital and axial ligand, the intensity and the energy of the peak A provide a measure for probing a local structure around the manganese ion. In fact, a very strong peak A is observed at around 6546 eV for tetragonal spinel or monoclinic layered lithium manganese oxides,[3,13] in which the trivalent manganese ion is commonly stabilized in the tetragonally distorted octahedra (Figure 2). This is due to the fact that the elongation of $Mn-O_{ax}$ bond facilitates the metal-to-ligand electron transfer along the *c*-axis and hence the shakedown process.[24] As can be seen clearly from the inset of Figure 2, the intensity of the peak A becomes smaller with increasing Cr content, underlining the shrinkage of the average $Mn-O_{ax}$ bond distance and the depression of the tetragonal distortion. This is consistent with the increase of Mn oxidation state, giving rise to the decrease of Jahn−Teller (JT) active Mn^{+III} concentration.

The local crystal structure of $LiMn_{2-x}Cr_xO_4$ has been quantitatively determined by EXAFS spectroscopy. The k^3-weighted Mn K-edge EXAFS spectra for $LiMn_{2-x}Cr_xO_4$ ($x =$ 0, 0.2, and 0.5) are presented in Figure 3, together with their Fourier transforms (FTs). All the spinel lithium manganates exhibit two intense FT peaks at ∼1.5 and ∼2.5 Å, which are attributed to Mn−O and Mn−M shells (M = Mn or Cr), respectively. As the manganese ion is replaced by the chromium ion, the intensities of both FT peaks become enhanced. Judging from the average Mn oxidation state of ∼+3.5 and the charge separation of the manganese in the spinel $LiMn_2O_4$,[16,17] there would be three different manganese−oxygen bond distances, i.e., $R(Mn^{+III}-O_{eq})$, $R(Mn^{+III}-O_{ax})$, and $R(Mn^{+IV}-O)$. Taking

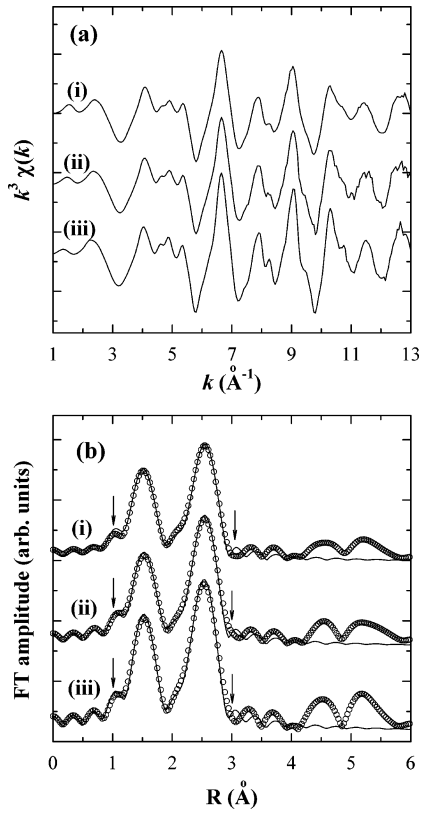

Figure 3. (a) k^3-weighted Mn K-edge EXAFS spectra and (b) their Fourier transforms for the cubic spinel $LiMn_{2-x}Cr_xO_4$ compounds with Cr content (x) of (i) 0, (ii) 0.2, and (iii) 0.5, respectively. The Fourier filtering range is shown by the arrows. The solid lines and empty circles represent the fitted and experimental data, respectively.

into account the fact that the longest $Mn^{+III}-O_{ax}$ bond would contribute to the damping of EXAFS signal,[3] the enhancement of FT peaks upon Cr substitution evidences the presence of the dynamic local tetragonal distortion around the manganese in $LiMn_{2-x}Cr_xO_4$ and the decrease of JT active Mn^{+III} ion concentration. To confirm the variation of the tetragonal distortion upon Cr substitution, we have performed a nonlinear curve fitting analysis. Among the three manganese−oxygen bonds in $LiMn_{2-x}Cr_xO_4$, $Mn^{+III}-O_{eq}$ and $Mn^{+IV}-O$ possess nearly the same bond distances of ∼1.91 Å but $Mn^{+III}-O_{ax}$ has a much greater bond distance of ∼2.32 Å.[16] By setting the two shorter Mn−O bonds as identical, we were able to construct a (5:1:6) model for $LiMn^{+IV}Mn^{+III}O_4$, in which there exist four $Mn^{+III}-O_{eq}$, six $Mn^{+IV}-O$, two $Mn^{+III}-O_{ax}$, and twelve Mn−Mn bonds.[25] In this way, we have also built (5.11:0.89:6) and (5.33:0.67:6) models for $LiMn^{+IV}Mn^{+III}_{0.8}Cr^{+III}_{0.2}O_4$ and $LiMn^{+IV}Mn^{+III}_{0.5}Cr^{+III}_{0.5}O_4$, respectively. With these models, we were able to obtain excellent fitting results to the experimental spectra, as shown in Figures 3b and 4. The fitted structural parameters are summarized in Table 2. The residual F^2 values were found to be quite smaller with the multiple Mn−O bond models than with the single Mn−O bond models constructed from the average crystal structure.[26] This confirms the presence of the local tetragonal distortion and the depression of this distortion upon chromium substitution, which is well correlated with the spectral variation in XANES region.

From the present XANES/EXAFS results, it becomes certain that there are two kinds of the Mn local symmetries corresponding to Mn^{+III} and Mn^{+IV} oxidation states in the spinel $LiMn_{2-x}Cr_xO_4$ and the replacement of Mn with Cr results in the decrease of the dynamic tetragonal distortion around Mn.

TABLE 2: Results of Nonlinear Least-Squares Curve-Fitting Analysis for the Mn K-Edge EXAFS Spectra of the Cubic Spinel $LiMn_{2-x}Cr_xO_4$ Compounds

sample	bond	CN	R (Å)	σ^2 ($10^{-3} \times$ Å^2)
$LiMn_2O_4$[a]	Mn−O_{eq}	5	1.90	3.68
	Mn−O_{ax}	1	2.33	8.69
	Mn−Mn	6	2.91	5.21
$LiMn_{1.8}Cr_{0.2}O_4$[a]	Mn−O_{eq}	5.89	1.91	3.59
	Mn−O_{ax}	1.11	2.34	13.46
	Mn−Mn,Cr	6	2.90	4.40
$LiMn_{1.5}Cr_{0.5}O_4$[a]	Mn−O_{eq}	5.33	1.90	3.19
	Mn−O_{ax}	0.67	2.34	10.68
	Mn−Mn,Cr	6	2.89	4.52

[a] The curve fitting analysis was performed for the range of $1.012 - R - 3.007$ Å and $3.75 - k - 13.00$ Å^{-1}.

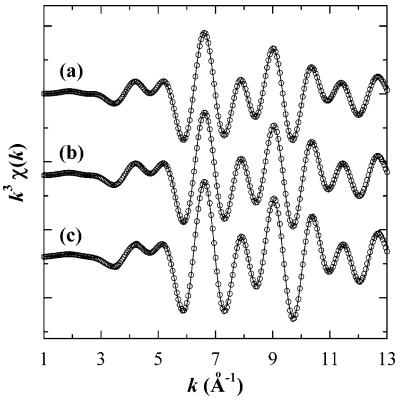

Figure 4. Fourier-filtered Mn K-edge EXAFS spectra for the cubic spinel $LiMn_{2-x}Cr_xO_4$ compounds with Cr content (x) of (a) 0, (b) 0.2, and (c) 0.5, respectively. The solid lines and empty circles represent the fitted and experimental data, respectively.

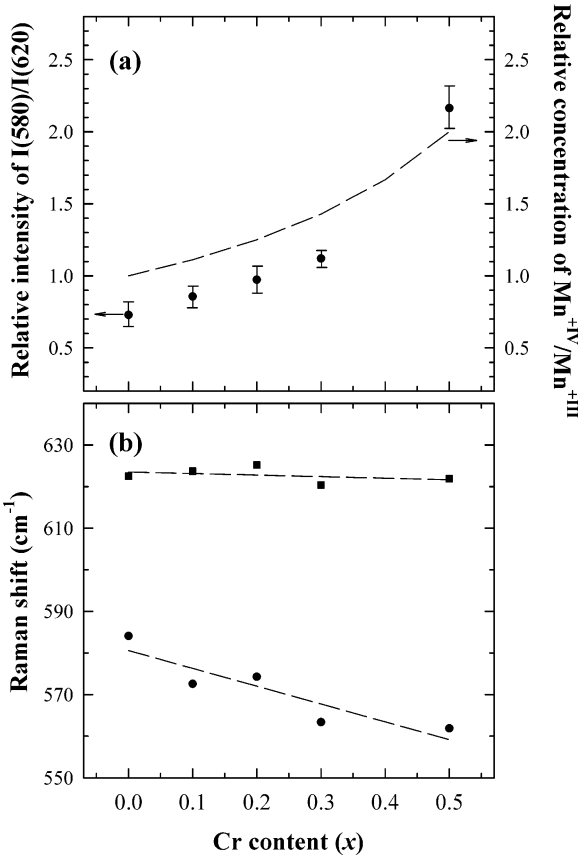

Figure 5. (a) Plot of the relative intensity ratio of two main peaks at ∼580 and ∼620 cm^{-1} (closed circles) and the calculated ratio of Mn^{+III}/Mn^{+IV} concentration (dashed lines). (b) Variation of the frequency of two main peaks at ∼580 (closed circles) and ∼620 cm^{-1} (closed squares) upon Cr substitution. The dashed lines obtained from an interpolation are guides for eyes.

On the basis of this experimental finding, we have assigned two intense Raman features at ∼580 and ∼620 cm^{-1} as A_{1g} modes for regular $Mn^{+IV}O_6$ octahedra and tetragonally distorted $Mn^{+III}O_6$ octahedra, respectively. This new assignment is supported from the fact that the cubic spinel λ-$Mn^{+IV}O_2$ and the tetragonal spinel $Li_2Mn^{+III}{}_2O_4$ show only one intense A_{1g} phonon line at 586 and 605 cm^{-1}, respectively (Figure 1). Slight differences in the peak frequency between the above references and $LiMn_2O_4$ can be explained by the dissimilar Mn oxidation state. To further verify the validity of the present peak assignment, we have plotted the ratio of peak area as a function of Cr content (x), in comparison with the relative concentration of Mn^{+IV}/Mn^{+III}. As shown in Figure 5a, the relative intensity of both peaks is rather consistent with the ratio of Mn^{+IV}/Mn^{+III} concentration, supporting the present peak assignment. In fact, previously, the intensity ratio of both peaks has been utilized to estimate the lithium content (y) in the spinel $Li_yMn_2O_4$,[12] implicating the relationship between the relative intensity of both peaks and the ratio of Mn^{+IV}/Mn^{+III} concentration. On the other hand, in contrast to the Cr-substituted cubic spinel $LiMn_{2-x}Cr_xO_4$ with mixed Mn valences, only one intense A_{1g} peak was reported for the tetragonal spinel $Li_2Mn^{+III}{}_{1.8}Cr_{0.2}O_4$ with a trivalent Mn oxidation state.[14] This allows us to conclude that the spectral feature of A_{1g} phonon line in the spinel-structured lithium manganate depends on the average oxidation state of manganese rather than the existence of chromium substituent. In contrast to the intense A_{1g} phonon line, a very diffuse and broad shape of weak $T_{2g}(1)$ and $T_{2g}(2)$ phonon lines in $LiMn_{2-x}Cr_xO_4$ would hinder the clear observation of peak splitting caused by the mixed Mn oxidation state. In addition, the remaining $T_{2g}(3)$ phonon line is believed to be concealed by the intense A_{1g} peak because the theoretical calculation for phonon frequency predicts nearly identical vibration frequencies for both phonon modes.[10]

As plotted in Figure 5b, the displacement of Mn with Cr has a different influence on the frequencies of two A_{1g} peaks; the peak at ∼580 cm^{-1} shows a small frequency shift upon Cr substitution whereas there is a negligible position change for the peak at ∼620 cm^{-1}. This indicates that the effect of Cr substitution is more prominent for the chemical environment of Mn^{+IV} ion than that of Mn^{+III} one. Taking into account the electrostatic repulsion between cations in the edge-shared octahedra, it is energetically favorable that a tetravalent Mn^{+IV} ion has a trivalent cation neighbor rather than a tetravalent one. Therefore, most of the substituted Cr^{+III} ion would exist around the Mn^{+IV} ion. In this case, the effect of Cr substitution is expected to be greater for the local structure around Mn^{+IV} ion, explaining the observed small shift of the 580 cm^{-1} phonon line toward the low-frequency side. As illustrated in Figure 6, the replacement of the longer Mn^{+III}−O_{ax} bond with the shorter Cr^{+III}−O one gives rise to the weakening of adjacent Mn^{+IV}−O bond through the bond competition along the π-channel. As a result, the phonon frequency of A_{1g} mode of $Mn^{+IV}O_6$ is decreased. In fact, such a decrease of A_{1g} mode frequency upon Cr substitution was also observed for the tetragonal spinel compound, i.e., 605 cm^{-1} for $Li_2Mn_2O_4$ and 600 cm^{-1} for Li_2-$Mn_{1.8}Cr_{0.2}O_4$.[14]

In summary, on the basis of the dynamic local structural information obtained from XANES/EXAFS analysis, we were able to re-interpret the Raman spectrum of the spinel lithium manganate and to understand the Raman spectral change induced

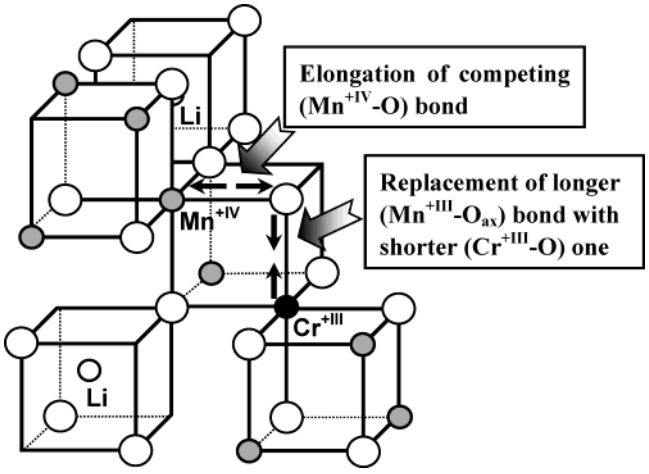

Figure 6. Schematic model for the effect of Cr substitution on the local crystal structure in cubic spinel $LiMn_{2-x}Cr_xO_4$ compound. Small black circles are Cr^{+III} ions, small gray circles are Mn^{+IV} ions, small open circles are Li^+ ions, and large open circles are O^{-II} ions.

by Cr substitution. This interpretation was further evidenced not only by the comparison with the reference spectra of $Li_2Mn_2O_4$ and λ-MnO_2 but also by the good correlation between the ratio of Mn^{+IV}/Mn^{+III} concentration and the relative intensities of two Raman peaks. Through the present study, it was clearly demonstrated that the Raman spectra reflect sensitively the dynamic local atomic arrangement rather than the static average crystal structure. Furthermore, we have established that the relative intensity of the two main Raman peaks of the spinel lithium manganate can be used as a measure for estimating the local symmetry and the oxidation state of manganese ion in the spinel lattice.

Acknowledgment. This work was supported by grant No. R08-2003-000-10409-0 from the Basic Research Program of the Korea Science & Engineering Foundation. We are grateful to Dr. P. V. Huong (University Bordeaux I), Dr. C. W. Kwon (University Bordeaux I), and Prof. J. B. Joo (Hanyang University Korea) for micro-Raman measurements and to Prof. M. Nomura for helping us to get the XAS data in the Photon Factory.

References and Notes

(1) Thackeray, M. M. *Prog. Solid State Chem.* **1997**, *25*, 1 and the references therein.

(2) Gummow, R. J.; de Kock, A.; Thackeray, M. M. *Solid State Ionics* **1994**, *69*, 59.

(3) Hwang, S. J.; Park, H. S.; Choy, J. H.; Campet, G. *J. Phys. Chem. B* **2001**, *105*, 335.

(4) (a) Sun, Y. K.; Jeon, Y. S.; Lee, H. J. *Electrochem. Solid State Lett.* **2000**, *3*, 361. (b) Palacin, M. R.; Le Cras, F.; Seguin, L.; Anne, M.; Chabre, Y.; Tarascon, J. M.; Amatucci, G.; Vaughan, G.; Strobel, P. *J. Solid State Chem.* **1999**, *144*, 361.

(5) (a) Hosoya, M.; Ikuta, H.; Wakihara, M. *Solid State Ionics* **1998**, *111*, 153. (b) Pistoia, G.; Antonini, A.; Rosati, R.; Bellitto, C.; Ingo, G. M. *Chem. Mater.* **1997**, *9*, 1443.

(6) (a) Oikawa, K.; Kamiyama, T.; Iziumi, F.; Nakazato, D.; Ikuta, H.; Wakihara, M. *J. Solid State Chem.* **1999**, *146*, 322. (b) Berg, H.; Thomas, J. O.; Liu, W.; Farrington, G. C. *Solid State Ionics* **1998**, *112*, 165.

(7) Treuil, N.; Labrugère, C.; Menetrier, M.; Portier, J.; Campet, G.; Deshayes, A.; Frison, J. C.; Hwang, S. J.; Song, S. W.; Choy, J. H. *J. Phys. Chem. B* **1999**, *103*, 2100.

(8) (a) Stoyanova, R. K.; Zhecheva, E. N.; Gorova, M. Y. *J. Mater. Chem.* **2000**, *10*, 1377. (b) Suzuki, S.; Tomita, M.; Okada, S.; Arai, H. *J. Phys. Chem. Solids* **1996**, *57*, 1851. (c) Zhecheva, E.; Stoyanova, R. *Solid State Ionics* **1993**, *66*, 143.

(9) (a) Morgan, K. R.; Collier, S.; Burns, G.; Ooi, K. *Chem. Commun.* **1994**, 1719. (b) Mustarelli, P.; Massarotti, V.; Bini, M.; Capsoni, D. *Phys. Rev. B* **1997**, *55*, 12018.

(10) (a) Ammundsen, B.; Burns, G. R.; Islam, M. S.; Kanoh, H.; Rozière, J. *J. Phys. Chem. B* **1999**, *103*, 5175. (b) Kanoh, H.; Tang, W.; Ooi, K. *Electrochem. Solid State Lett.* **1998**, *1*, 17.

(11) Huang, W.; Trech, R. *J. Power Sources* **1999**, *81*−*82*, 616.

(12) Hwang, S. J.; Park, H. S.; Choy, J. H.; Campet, G.; Portier, J.; Kwon, C. W.; Etourneau, J. *Electrochem. Solid State Lett.* **2001**, *4*, A213−A216.

(13) Hwang, S. J.; Park, H. S.; Choy, J. H.; Campet, G. *J. Phys. Chem. B* **2000**, *104*, 7612.

(14) Hwang, S. J.; Park, H. S.; Choy, J. H. *Solid State Ionics* **2002**, *151*, 275.

(15) Hwang, S. J.; Kwon, C. W.; Portier, J.; Campet, G.; Park, H. S.; Choy, J. H.; Huong, P. V.; Yoshimura, M.; Kakihana, M. *J. Phys. Chem. B* **2002**, *106*, 4053.

(16) Yamaguchi, H.; Yamada, A.; Uwe, H. *Phys. Rev. B* **1998**, *58*, 8.

(17) Shiraishi, Y.; Nakai, I.; Tsubata, T.; Himeda, T.; Nishikawa, F. *J. Solid State Chem.* **1997**, *133*, 587.

(18) Shannon, R. D. *Acta Crystallogr. A* **1976**, *32*, 751.

(19) Oyanagi, H.; Matsushida, T.; Ito, M.; Kuroda, H. *KEK Rep.* **1984**, *83*, 30.

(20) Choy, J. H.; Hwang, S. J.; Park, N. G. *J. Am. Chem. Soc.* **1997**, *119*, 1624.

(21) The present spectrum of cubic spinel $LiMn_2O_4$ sample prepared by a slow cooling process was found to be rather different from the previously reported one obtained from the sample prepared by the rapid quenching process.[12] Such differences would be ascribed to the presence of oxygen defect, because the deviation from stoichiometry was known to induce significant spectral variation.[11]

(22) We have also examined the electronic configuration and local symmetry of chromium and found that all the Cr-containing compounds under investigation possess a trivalent Cr^{+III} oxidation state with a regular octahedral symmetry.

(23) Horne, C. R.; Bergmann, U.; Grush, M. M.; Perera, R. C. C.; Ederer, D. L.; Callcott, T. A.; Cairns, E. J.; Cramer, S. P. *J. Phys. Chem. B* **2000**, *104*, 9587.

(24) Choy, J. H.; Kim, D. K.; Hwang, S. H.; Demazeau, G. *Phys. Rev. B* **1994**, *50*, 16631.

(25) Due to the limited numbers of allowed variables for the present data range, we constrained all the Mn−Mn bond distances to be identical, as in ref 16. This constraint can be rationalized from the fact that the Mn^{+IV}−Mn^{+IV} bond distance is similar to the average value of two kinds of Mn^{+III}−Mn^{+III} bond distances.

(26) With the multiple Mn−O bond models, the best-fit residual F^2 factors ($=\Sigma\{k^3(\chi(k)_{cal} - \chi(k)_{exp})\}^2/(n-1)$) were determined to be 0.028 for $LiMn_2O_4$, 0.048 for $LiMn_{1.8}Cr_{0.2}O_4$, and 0.075 for $LiMn_{1.5}Cr_{0.5}O_4$, respectively. These values are markedly smaller than the F^2 factors obtained from the single Mn−O bond models (0.090 for $LiMn_2O_4$, 0.084 for $LiMn_{1.8}Cr_{0.2}O_4$, and 0.232 for $LiMn_{1.5}Cr_{0.5}O_4$).